PHYSICAL REVIEW A **96**, 012514 (2017)

Theoretical study of the hyperfine-interaction constants and the isotope-shift factors for the $3s^2\,{}^1S_0$–$3s3p\,{}^{3,1}P_1^o$ transitions in Al^+

Tingxian Zhang,[1,2] Luyou Xie,[1] Jiguang Li,[2,*] and Zehuang Lu[3]

[1]*College of Physics and Electronic Engineering, Northwest Normal University, Lanzhou 730070, People's Republic of China*
[2]*Institute of Applied Physics and Computational Mathematic, Beijing 100088, People's Republic of China*
[3]*MOE Key Laboratory of Fundamental Physical Quantities Measurement, School of Physics, Huazhong University of Science and Technology, Wuhan 430074, People's Republic of China*

(Received 13 April 2017; published 21 July 2017)

We calculated the magnetic dipole and the electric quadrupole hyperfine interaction constants of $3s3p\,{}^{3,1}P_1^o$ states and the isotope shift, including mass and field shift, factors for transitions from these two states to the ground state $3s^2\,{}^1S_0$ in Al^+ ions using the multiconfiguration Dirac-Hartree-Fock method. The effects of the electron correlations and the Breit interaction on these physical quantities were investigated in detail based on the active space approach. It is found that the core-core and the higher order correlations are considerable for evaluating the uncertainties of the atomic parameters concerned. The uncertainties of the hyperfine interaction constants in this work are less than 1.6%. Although the isotope shift factors are highly sensitive to the electron correlations, reasonable uncertainties were obtained by exploring the effects of the electron correlations. Moreover, we found that the relativistic nuclear recoil corrections to the mass shift factors are very small and insensitive to the electron correlations for Al^+. These atomic parameters present in this work are valuable for extracting the nuclear electric quadrupole moments and the mean-square charge radii of Al isotopes.

DOI: 10.1103/PhysRevA.96.012514

I. INTRODUCTION

The exotic nuclei and the nuclei close to the drip line have some peculiar structures and properties, such as larger nuclear radii and reaction cross section, etc. Investigating the properties of these nuclei, especially for the evolutionary trend of the nuclear properties along the isotope chain, is helpful for understanding the many-body interactions within the nucleus and improving the nuclear structure theory [1]. To characterize the nuclear properties quantitatively, nuclear electric quadrupole moment Q and mean-square charge radius $\langle r^2\rangle$ are required. In the chain of aluminum isotopes, the proton-rich isotope ${}^{23}\mathrm{Al}$ has the proton-halo structure [2,3], the neutron-rich isotopes ${}^{31-33}\mathrm{Al}$ are in the vicinity of the "island of inversion", and the ${}^{26}\mathrm{Al}$ is a self-conjugate nucleus [4]. To date, the Q and $\langle r^2\rangle$ values have been available only for a few isotopes of aluminum, and the accuracies are not high enough except for ${}^{27}\mathrm{Al}$ [5–7]. For example, the Q value of ${}^{26}\mathrm{Al}$, with an uncertainty of about 12%, was deduced from the experimental hyperfine structures measured using atomic laser spectroscopy [8] in assistance of the relation ${}^{26}Q/{}^{27}Q = {}^{26}B/{}^{27}B$ (B is the electric quadrupole hyperfine interaction constants). For the ${}^{23}\mathrm{Al}$, ${}^{28}\mathrm{Al}$, and ${}^{31-33}\mathrm{Al}$ isotopes, the nuclear electric quadrupole moments were measured by the β-ray-detected nuclear magnetic resonance (β-NMR) or β-ray-detected nuclear quadrupole resonance (β-NQR) method [3,9–13]. However, the error bars, about 20% for ${}^{23}\mathrm{Al}$ and ${}^{31}\mathrm{Al}$, are so large that the nuclear deformation parameter β cannot be determined. Compared with the nuclear quadrupole moment, the nuclear charge mean square root is scarce. The $\langle r^2\rangle$ value of these interesting nuclei has not been reported. As a consequence, it is indispensable to determine accurately the Q and $\langle r^2\rangle$ values of aluminium isotopes for exploring their nuclear properties.

The nuclear-model-independent data Q and $\langle r^2\rangle$ can be extracted by combining the measured hyperfine structures and isotope shifts with theoretical prediction of the electric field gradient and the isotope shift factors. The collinear laser spectroscopy technique has been developed to measure the isotope shifts and the hyperfine structures of the exotic or radioactive nuclei with short lifetime and low production [1,14]. In addition, the high-precision measurements of hyperfine structures and isotope shifts of Al^+ ions can be obtained based on the Al^+ ion optical clock [15] and thus can be used to verify the calculation. For these reasons, the Al^+ ion can be considered as a good candidate for extracting the nuclear electric quadrupole moment Q and mean-square charge radius $\langle r^2\rangle$ of Al isotopes.

Most of the earlier theoretical works related to the $3s3p\,{}^{1,3}P_1^o$–$3s^2\,{}^1\mathrm{S}_0$ transitions in Al^+ ions focused on transition energies and probabilities [16–30]. For the hyperfine interaction constants, we only found theoretical reports by Kang *et al.* and Andersson *et al.* In their works, the off-diagonal magnetic dipole and electric quadrupole hyperfine interaction constants of the $3s3p\,{}^{1,3}P_1^o$ states were calculated for investigating the effect of hyperfine interaction on the lifetime of metastable states $3s3p\,{}^3P_{0,2}^o$ [28,30]. While the isotope shift factors of the transitions $3s3p\,{}^{1,3}P_1^o$–$3s^2\,{}^1S_0$ for Al^+ ions have not been reported.

In this work, we calculated the hyperfine interaction constants of $3s3p\,{}^{3,1}P_1^o$ states and the mass shift and field shift factors of the $3^2\,{}^1S_0$–$3s3p^{3,1}\,P_1^o$ in Al^+ using the multiconfiguration Dirac-Hartree-Fock (MCDHF) method. The active space approach was adopted to investigate the effects of electron correlations on the hyperfine interaction constants and the isotope shift factors in detail. Based on this, we built a computation model which can capture electron correlations effectively and allow us to obtain high-precision atomic parameters concerned. In addition, the relativistic nuclear recoil corrections to the isotope shift factors were

---

[*] li_jiguang@iapcm.ac.cn

discussed. We hope this work could support the experimental investigations about the Al^+ ion optical clock and the studies about the nuclear properties of Al isotopes.

II. THEORETICAL METHOD

A. MCDHF method

In the MCDHF method, an atomic state wave function (ASF) Ψ is a linear combination of configuration state functions (CSFs) Φ with the same parity P, total angular momentum J, and its component along the z direction M_J [31],

$$\Psi(\gamma PJM_J) = \sum_{i=1}^{N_{\mathrm{CSF}}} c_i \Phi(\gamma_i PJM_J). \tag{1}$$

In Eq. (1), c_i is the mixing coefficient and γ represents other appropriate labeling of the CSF. The CSFs are the linear combinations of products of one-electron Dirac orbitals. In the self-consistent field (SCF) calculation, both the mixing coefficients and the orbital are optimized. After the virtual orbital set is obtained, more electron correlations can be included in the relativistic configuration interaction (RCI) calculations by further expanding the configuration space. In the RCI calculations, all orbitals are kept frozen, and only the mixing coefficients are variable. The Breit interaction in the low-frequency approximation,

$$B_{ij} = -\frac{1}{2r_{ij}}\left[\boldsymbol{\alpha}_i \cdot \boldsymbol{\alpha}_j + \frac{(\boldsymbol{\alpha}_i \cdot \boldsymbol{r}_{ij})(\boldsymbol{\alpha}_j \cdot \boldsymbol{r}_{ij})}{r_{ij}^2}\right], \tag{2}$$

is also taken into account in the RCI computation [32].

B. Hyperfine interaction

The hyperfine interaction is caused by the interaction between the electrons and the electromagnetic multipole moments of the nucleus, and its Hamiltonian can be represented using the spherical tensor operators $\boldsymbol{T}^{(k)}$ and $\boldsymbol{M}^{(k)}$ [33],

$$H_{\mathrm{hfs}} = \sum_{k\geqslant 1} \boldsymbol{T}^{(k)} \cdot \boldsymbol{M}^{(k)}. \tag{3}$$

Here, $k=1$ and $k=2$ represent the magnetic dipole and electric quadrupole interactions, respectively, and the higher order terms are tiny and neglected in this work. For an N-electron atom, the electronic tensor operators $\boldsymbol{T}^{(1)}$ and $\boldsymbol{T}^{(2)}$ are the sums of the one-electron operators,

$$\boldsymbol{T}^{(\mathbf{1})} = \sum_{j=1}^{N} \boldsymbol{t}^{(1)}(j) = \sum_{j=1}^{N} -i\alpha[\boldsymbol{\alpha}_j \cdot \mathbf{l}_j \boldsymbol{C}^{(1)}(j)]r_j^{-2} \tag{4}$$

and

$$\boldsymbol{T}^{(\mathbf{2})} = \sum_{j=1}^{N} \boldsymbol{t}^{(2)}(j) = \sum_{j=1}^{N} -\boldsymbol{C}^{(2)}(j)r_j^{-3}. \tag{5}$$

Here, i is the imaginary unit, α is the fine-structure constant, $\boldsymbol{C}^{(1)}$ and $\boldsymbol{C}^{(2)}$ are spherical tensor operators, and $\mathbf{l}$ is the orbital angular momentum operator. The nuclear tensor operators $\boldsymbol{M}^{(1)}$ and $\boldsymbol{M}^{(2)}$ are related to magnetic dipole moment μ_I and electronic quadrupole moment Q of the nucleus with spin I through [34]

$$\mu_I = \langle IM_I(=I)|\boldsymbol{M}_0^{(1)}|IM_I(=I)\rangle \tag{6}$$

and

$$Q = \langle IM_I(=I)|\boldsymbol{M}_0^{(2)}|IM_I(=I)\rangle. \tag{7}$$

In the first-order perturbation approximation, the magnetic dipole and the electric quadrupole hyperfine interaction constants A_J and B_J are [34]

$$A_J = \frac{\mu_I}{I}\frac{1}{[J(J+1)]^{1/2}}\langle\Psi(PJ)\|\boldsymbol{T}^{(1)}\|\Psi(PJ)\rangle \tag{8}$$

and

$$B_J = 2Q\left[\frac{J(2J-1)}{(J+1)(2J+3)}\right]^{1/2}\langle\Psi(PJ)\|\boldsymbol{T}^{(2)}\|\Psi(PJ)\rangle. \tag{9}$$

C. Isotope shifts

The isotope shift is composed of the mass shift (MS) and the field shift (FS). The former is caused by the motion of nucleus with finite mass and the latter by the nuclear distribution. For a transition, the isotope shift is

$$\Delta E_{\mathrm{IS}}^{A,A'} = \Delta E_{\mathrm{MS}}^{A,A'} + \Delta E_{\mathrm{FS}}^{A,A'} \tag{10}$$

$$= \left(\frac{1}{M} - \frac{1}{M'}\right)\Delta K_{\mathrm{RMS}} + \Delta F \delta\langle r^2\rangle^{A,A'}. \tag{11}$$

In the formulas above, the M and M' are the nuclear masses of the isotopes A and A', respectively. In addition, $\delta\langle r^2\rangle^{A,A'} \equiv \langle r^2\rangle^A - \langle r^2\rangle^{A'}$. The mass shift (MS) can be separated into the normal mass shift (NMS) and the specific mass shift (SMS). The relativistic nuclear recoil Hamiltonians H_{RNMS} and H_{RNMS} correspond to one-body and two-body relative mass shift operators, respectively [35,36],

$$H_{\mathrm{RMS}} = H_{\mathrm{RNMS}} + H_{\mathrm{RSMS}} \tag{12}$$

$$= \frac{1}{2M}\sum_i\left\{\boldsymbol{p}_i^2 - \frac{\alpha z}{r_i}\left[\boldsymbol{\alpha}_i + \frac{(\boldsymbol{\alpha}_i \cdot \boldsymbol{r}_i)\boldsymbol{r}_i}{r_i^2}\right]\cdot \boldsymbol{p}_i\right\} \tag{13}$$

$$+ \frac{1}{2M}\sum_{i\neq j}\left\{\boldsymbol{p}_i \cdot \boldsymbol{p}_j - \frac{\alpha z}{r_i}\left[\boldsymbol{\alpha}_i + \frac{(\boldsymbol{\alpha}_i \cdot \boldsymbol{r}_i)\boldsymbol{r}_i}{r_i^2}\right]\cdot \boldsymbol{p}_j\right\}. \tag{14}$$

For a given level, the normal mass shift factors K_{RNMS} and the specific mass shift factors K_{RSMS} are defined as [37]

$$K_{\mathrm{RNMS}} \equiv M\langle\Psi|H_{\mathrm{RNMS}}|\Psi\rangle \tag{15}$$

and

$$K_{\mathrm{RSMS}} \equiv M\langle\Psi|H_{\mathrm{RSMS}}|\Psi\rangle. \tag{16}$$

For a transition, the ΔK is the difference of the mass shift factors between the upper (u) and lower (l) levels, and $\Delta K_{\mathrm{RMS}} = \Delta K_{\mathrm{RNMS}} + \Delta K_{\mathrm{RSMS}}$.

The field shift (FS) factor for a given transition is expressed as [38]

$$\Delta F = \frac{2\pi}{3}\left(\frac{Ze^2}{4\pi\epsilon_0}\right)\Delta|\Psi(\mathbf{0})|^2, \tag{17}$$

where $\Delta|\Psi(\mathbf{0})|^2$ is the change of the total electronic probability density at the origin

$$\Delta|\Psi(\mathbf{0})|^2 = \Delta\rho^e(\mathbf{0}) = \rho_u^e(\mathbf{0}) - \rho_l^e(\mathbf{0}). \tag{18}$$

III. COMPUTATIONAL MODEL

Generally the precision of the calculated atomic parameters mainly depends on description of electron correlations in the atomic system. In the frame of the MCDHF method, one can consider electron correlations systematically, adopting the active space approach. According to the perturbation theory, the electron correlations can be divided into the first-order and the higher-order correlations. The first-order correlation effects are captured by the CSFs generated through the single (S) and double (D) excitations from the occupied orbitals in the single reference configuration (SR) sets. In order to capture the electron correlations efficiently, the occupied orbitals in the reference configuration are separated into the valence and the core orbitals. Therefore, the first-order correlation is composed of the correlation between the valence electrons (VV correlation), the correlation between valence and core electrons (CV correlation), and the correlation between core electrons (CC correlation). The one beyond the first-order correlation is defined as the higher-order correlation and captured by the configuration space expanding from the multireference (MR) configurations set, i.e., the MR-SD model. It was shown that this method is capable of accounting for the electron correlation for the complex ions and atoms [32,39–43].

A. Capture of the first-order correlations

In our calculations, the atomic state wave function of even $3s^2$ and odd $3s3p$ states were optimized separately. We treated the $1s$, $2s$, and $2p$ orbitals as the core, and the others as the valence orbitals. The VV and CV correlations were taken into account in the SCF calculations. As shown in the second column of Tables I and II, the active orbitals (AO) were enlarged layer by layer in order to monitor the convergence of the physical quantities concerned. These steps were labeled by CV_{1s}-nl, where the subscript $1s$ means the CV correlation between the $1s$ core and the valence orbitals was involved. n and l are the maximum principal quantum number and the maximum angular quantum number of the outermost active orbitals at each step, respectively. In our test calculations, it was found that the contributions from orbitals with large orbital angular momentum l (such as $7i$, $7h$, $8g$ orbitals, etc.) are fractional to the atomic parameters concerned, so these orbitals were not included in the set of active orbitals. The final set of active orbitals in our calculations was composed of eleven layers of orbitals with $l \leqslant 2$, seven layers with $l = 3$, three layers with $l = 4$, and one layer with $l = 5$. The number of CSFs for $3s^2$ and $3s3p$ states in each step are also presented in Tables I and II. The SCF calculations started from the Dirac-Hartree-Fock approximation (labeled as DF in the table), in which the occupied orbitals in the reference configurations were optimized as spectroscopic. Subsequently, these orbitals were kept frozen, and only the added orbitals in the active set were variable. At last, the orbitals sets formed in the step CV_{1s}-$13d$ were fixed in subsequent RCI calculations in which the CC_{2s} and the higher-order correlations were included.

The correlation in the $n = 2$ core (labeled as CC_{2s}) was taken into account by allowing the single and double excitations from the $2s$ and $2p$ core orbitals to the largest active set. So far, all the first-order correlations were included in our calculations except the correlation between the core orbitals 1s (CC_{1s} correlation). In fact, the CC_{1s} correlation is negligible and will be discussed in section below.

B. Capture of the higher-order correlations

The higher-order correlation can be captured in two ways. One is to add the CSFs generated by the triple (T) and quadruple (Q) substitutions from the single reference configuration, and the other is to include those produced through the SD substitutions from the multireference configurations. The first way is impracticable for complex atoms, since the configuration

TABLE I. The number of CSFs for the ground state $3s^2$ in various correlation models. AO represents the active orbitals in different calculation models, and NCSF is the number of CSFs.

Reference configurations	AO($n_{\mathrm{max}}l$)	Model	NCSF $J^p = 0^e$
$2s^22p^63s^2$		DF	1
	$4s, 3p, 3d, 4f$	CV_{1s}-$4f$	61
	$5s, 4p, 4d, 5f, 5g$	CV_{1s}-$5g$	254
	$6s, 5p, 5d, 6f, 6g, 6h$	CV_{1s}-$6h$	616
	$7s, 6p, 6d, 7f, 7g, 6h$	CV_{1s}-$7g$	1098
	$8s, 7p, 7d, 8f, 7g, 6h$	CV_{1s}-$8f$	1603
	$9s, 8p, 8d, 9f, 7g, 6h$	CV_{1s}-$9f$	2211
	$10s, 9p, 9d, 10f, 7g, 6h$	CV_{1s}-$10f$	2922
	$11s, 10p, 10d, 10f, 7g, 6h$	CV_{1s}-$11d$	3509
	$12s, 11p, 11d, 10f, 7g, 6h$	CV_{1s}-$12d$	4163
	$13s, 12p, 12d, 10f, 7g, 6h$	CV_{1s}-$13d$	4884
	$13s, 12p, 12d, 10f, 7g, 6h$	CC_{2s}	14988
$+2s^22p^63p^2$	$8s, 8p, 7d, 8f, 7g, 6h$	MR_1-8	23358
$+2s^22p^43s^24p^2$; $2s^22p^43s^23d^2$; $2s^22p^53s3p3d$	$6s, 7p, 6d, 6f, 6g, 6h$	MR_2-6	229659
$+2s^22p^43s^23p4p$; $2s^22p^43s^23d4d$; $2s2p^53s^24s4p$; $2s^22p^43s^24p5p$	$5s, 6p, 5d, 4f, 5g$	MR_3-5	357223

TABLE II. The number of CSFs for the excited states $3s3p$ in various correlation models. AO represents the active orbitals in different calculation models, and NCSF is the number of CSFs.

Reference configurations	AO($n_{\max}l$)	Model	NCSF $J^p = 1^o$
$2s^22p^63s3p$		DF	2
	$4s, 4p, 3d, 4f$	CV$_{1s}$-$4f$	600
	$5s, 5p, 4d, 5f, 5g$	CV$_{1s}$-$5g$	2326
	$6s, 6p, 5d, 6f, 6g, 6h$	CV$_{1s}$-$6h$	5573
	$7s, 7p, 6d, 7f, 7g, 6h$	CV$_{1s}$-$7g$	9860
	$8s, 8p, 7d, 8f, 7g, 6h$	CV$_{1s}$-$8f$	14292
	$9s, 9p, 8d, 9f, 7g, 6h$	CV$_{1s}$-$9f$	19594
	$10s, 10p, 9d, 10f, 7g, 6h$	CV$_{1s}$-$10f$	25766
	$11s, 11p, 10d, 10f, 7g, 6h$	CV$_{1s}$-$11d$	30696
	$12s, 12p, 11d, 10f, 7g, 6h$	CV$_{1s}$-$12d$	36146
	$13s, 13p, 12d, 10f, 7g, 6h$	CV$_{1s}$-$13d$	42116
	$13s, 13p, 12d, 10f, 7g, 6h$	CC$_{2s}$	223468
$+2s^22p^63p3d$	$8s, 8p, 8d, 8f, 7g, 6h$	MR$_1$-8	352702
$+2s^22p^63s5p$; $2s^22p^63s4p$; $2s^22p^63d5p$	$5s, 7p, 5d, 5f, 5g$	MR$_2$-5	400690
$+2s^22p^43s3p4p^2$; $2s^22p^43s3p4d^2$	$4s, 6p, 5d, 4f$	MR$_3$-4	1327012

space will be expanded too rapidly. Moreover, it is unnecessary to capture all TQ substitutions in practical calculations, because the contributions from most of them are tiny. Actually, the SD excitations from the multireference configuration set is equivalent to the restricted TQ excitations from the single reference configuration, but reserve the important TQ excitations by properly selecting the reference configurations. Therefore, the most important higher order correlation can be captured by using the MR-SD model. From the physical viewpoint, the multireference configuration set is composed of the CSFs with large mixing coefficient in the first-order configuration space. In this case, we selected the dominant CSFs in the configuration spaces obtained with the CC$_{2s}$ model to form the multireference configuration set, since the contributions of the CC$_{1s}$ correlations to the mixing coefficient of the dominant CSFs are negligible. The dominant CSFs can be identified according to the weight factor that is defined as

$$\omega = \left(\sum_i c_i^2\right)^{1/2}. \tag{19}$$

Here, the sum extends over the CSFs that belong to the same configuration [41]. Table III shows the weight of the selected configurations. It should be noted that the weight factors in this table were obtained by summing the configuration with $c_i > 0.01$, because the mixing coefficients $c_i < 0.01$ only have tiny effects on the calculated weight factor of the configuration.

In order to explore the convergency of the higher order correlation effect, we expanded the multireference configuration set in terms of the conditions $\omega > 0.05$, $\omega > 0.02$, and $\omega > 0.01$, i.e., the MR$_1$, MR$_2$, and MR$_3$ sets in Table III, respectively. It should be emphasized that only the higher order correlation between valence orbitals ($3s$ and $3p$) and the $n = 2$ core orbitals ($2s$ and $2p$) was considered in our calculations. In addition, in order to ensure the convergency of the atomic parameters concerned for a given MR set, the orbitals in the active set were added layer by layer as mentioned earlier. For example, five layers of correlation orbitals were added for capturing adequately the higher order correlation under the condition of $\omega > 0.05$. This was marked as MR$_1$-8, in which 8 is the maximum principal quantum number of the active s orbitals for the corresponding MR$_1$ model. Similar regulation was used for the MR$_2$ and MR$_3$ models as well. Moreover, we should point out that in the selection of the multireference configurations, we balanced the weights of the given configurations for $^3P_1^o$ and $^1P_1^o$ states since these levels

TABLE III. The weight factors ω of the configurations in multireference configurations (MR) for the $3s^2\,^1S_0$ and $3s3p\,^{3,1}P_1^o$ states.

Model	$3s^2\,^1S_0$ Configurations	ω	$3s3p\,^3P_1^o$ Configurations	ω	$3s3p\,^1P_1^o$ Configurations	ω
MR$_1$	$2s^22p^63s^2$	0.9810	$2s^22p^63s3p$	0.9896	$2s^22p^63s\,3p$	0.9781
	$2s^22p^63p^2$	0.1382	$2s^22p^63p3d$	0.0557	$2s^22p^63p3d$	0.1439
MR$_2$	$2s^22p^43s^23d^2$	0.0385	$2s^22p^63s5p$	0.0175	$2s^22p^63s5p$	0.0360
	$2s^22p^43s^24p^2$	0.0300	$2s^22p^63s4p$	0.0209	$2s^22p^63s4p$	0.0270
	$2s^22p^53s3p3d$	0.0204	$2s^22p^63d5p$	0.0085	$2s^22p^63d5p$	0.0262
MR$_3$	$2s^22p^43s^23p4p$	0.0179	$2s^22p^43s3p4d^2$	0.0194	$2s^22p^43s3p4d^2$	0.0188
	$2s^22p^43s^23d4d$	0.0162	$2s^22p^43s3p4p^2$	0.0160	$2s^22p^43s3p4p^2$	0.0111
	$2s2p^53s^24s4p$	0.0162				
	$2s^22p^43s^24p5p$	0.0158				

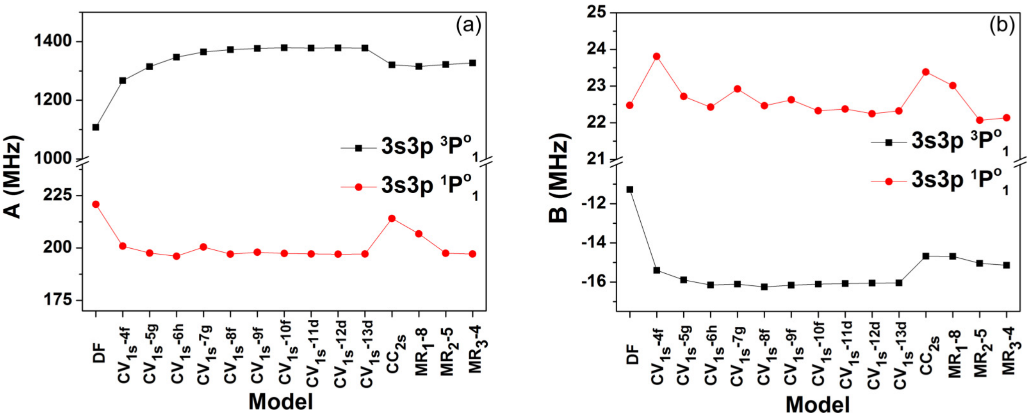

FIG. 1. The hyperfine interaction constants (in MHz) A (a) and B (b) of $3s3p\,^{3,1}P_1^o$ states in the Al^+ ion as functions of the computational models.

were optimized on a common orbital basis set. It means that the $2s\,^2 2p\,^6 3s5p$ and $2s\,^2 2p\,^6 3d5p$ were added in the MR_2 set, since their weights for $^1P_1^o$ state satisfy $\omega > 0.02$. At last, the contribution of the Breit interaction was evaluated in the DF model. The calculations in this work were carried out by using the GRASP2K code [44,45].

IV. RESULTS AND DISCUSSION

A. Hyperfine interaction constants of $3s3p\,^{3,1}P_1^o$

Figure 1 shows the magnetic dipole (A) and the electric quadrupole (B) hyperfine interaction constants of the $3s3p\,^{3,1}P_1^o$ states in Al^+ ions as functions of the configuration spaces. It can be seen that seven layers of correlation orbitals are enough to capture the VV and CV electron correlation effects in the SCF calculations. The extra three layers were augmented for adequately describing the core-core correlation in the subsequent RCI computation. In addition, the relatively large oscillation for the electric quadrupole hyperfine interaction constants of the $3s3p\,^1P_1^o$ state occurs because the scale in this figure is small. The contributions of CC_{2s} correlations to the A and B constants are −4% and −9% for the $^3P_1^o$ state, respectively, and 9% and 5% for the $^1P_1^o$ state. The higher-order correlation on the hyperfine interaction constants were accounted for by the MR_3-4 model. These contribute to the magnetic dipole and the electric quadrupole hyperfine interaction constants of the $^3P_1^o$ state by 0.6% and 3%, respectively, and of the $^1P_1^o$ state by −8% and −5%. It is worth noting that the higher order correlation effects counteract the core-core correlation effects. For instance, the effects of the CC_{2s} correlation on the magnetic dipole hyperfine interaction constants of the $^1P_1^o$ states are offset by the higher order correlation, so the final results obtained with the MR_3-4 model are in good agreement with the one from the CV_{1s}-13d models. In fact, Engles [46] and Jacek *et al.* [47] found this phenomenon in their works; that is, the CC correlations always make the agreement worse between the calculated hyperfine interaction constants and the experimental values, and these discrepancies can be offset by the higher order correlation. Hence, for the calculation asked for high precision, the CC correlation and the higher order correlation are indispensable, which also allows us to evaluate the uncertainties in the calculation.

TABLE IV. The off-diagonal hyperfine interaction constants (in MHz) between $3s3p\,^{3,1}P_1^o$ and $^3P_0^o$ (A_{30}, A_{10}), and between $3s3p\,^{3,1}P_1^o$ and $^3P_2^o$ ($A_{32}B_{32}$, $A_{12}B_{12}$). The results of Kang *et al.* and Andersson *et al.* in this table are converted from the hyperfine matrix elements W_{30} and W_{10} in the work of Kang *et al.* [28] and the reduced hyperfine interaction constants of the $3s3p$ in the work of Andersson *et al.* [30], respectively. The nuclear spin, the magnetic dipole, and the electric quadrupole moments of $^{27}\mathrm{Al}$, $I = 5/2$, $\mu_I = 3.6415069\mu_N$, $Q = 0.1466\mathrm{b}$ were taken from the table by Stone [48].

Author	A_{30}	A_{10}	A_{32}	A_{12}	B_{32}	B_{12}
This work	1309	1027	−537	826	7.50	−0.0121
Andersson [30]	1349	1071	−555	861	8.05	−0.0098
Kang [28]	1162	928				

Kang *et al.* and Andersson *et al.* [28,30] calculated the off-diagonal hyperfine interaction constants using the MCDHF method in order to investigate the influence of hyperfine interaction on the lifetime of metastable states $3s3p\,^3P_{0,2}^o$. To confirm our computation models are reliable, we made comparisons for the off-diagonal hyperfine interaction constants between our and their results in Table IV. As can be seen from this table, excellent agreement was found between our results and those of Andersson *et al.* The less good agreement with results of Kang *et al.* is caused by the fact that the core-valence correlation between the $1s$ orbitals and the valence orbitals, the core-core correlation, and the higher-order correlation were not considered in their calculation.

Table V shows the calculated hyperfine interaction constants corresponding to the MR_3-4 model and their uncertainties (in the parentheses) of the $3s3p\,^{3,1}P_1^o$ states in Al^+ ions.

TABLE V. The hyperfine interaction constants (in MHz) A and B of $3s3p\,^{3,1}P_1^o$ states in Al^+ ions. The results in the parentheses are the uncertainties for our results.

Model	$3s3p\,^3P_1^o$		$3s3p\,^1P_1^o$	
	A	B	A	B
MR_3-4	1327.3(10.2)	−15.1(0.2)	197.1(2.8)	22.1(0.3)

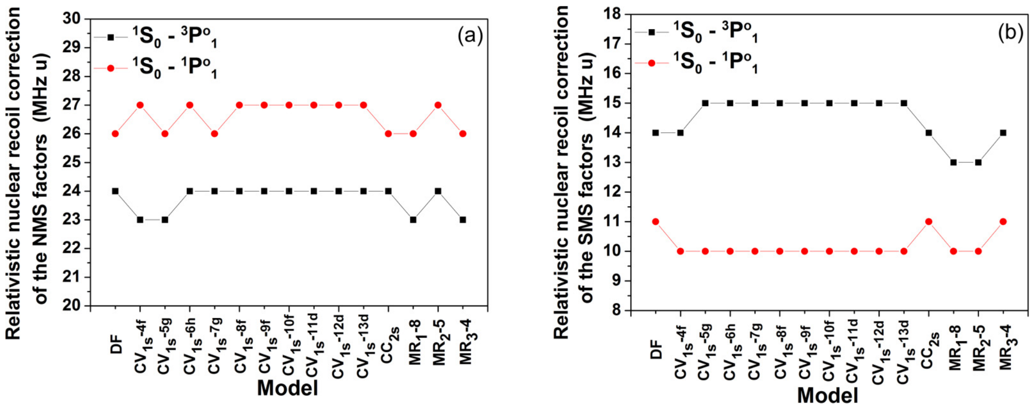

FIG. 2. The relativistic nuclear recoil corrections of the NMS (a) and SMS (b) factors for the transitions $3s^2\,^1S_0$–$3s3p\,^{3,1}P_1^o$ in the Al^+ ion as functions of the computational models.

Generally, the uncertainties result from electron correlations neglected in the computational models and physical effects. In this work the VV, CV_{1s}, CC_{2s}, and the main part of higher order correlations were taken into account systematically. According to the convergence trend illustrated in Fig. 2, there are around 0.8% uncertainties in the calculations. The CC_{1s} correlation and the higher order correlation involving the $1s$ orbital were neglected in our computational models. From our test, we found that the effects of the CC_{1s} correlations on the hyperfine interaction constants under investigation are less than 1%. As discussed above, the effects of the core-core correlation related to the $n = 2$ shell on the hyperfine interaction constants almost counteract the higher order correlation effects. We speculated that the cancellation also arises between the CC_{1s} and the related higher order correlation. Therefore, the uncertainty due to the neglected CC_{1s} and the higher order effects should be less than 1%. Additionally, the Breit interaction was ignored in the present calculation, which gives rise to 0.05% uncertainty. The total uncertainties of A and B are 0.77% and 1.32% for the $^3P_1^o$ state, and 1.42% and 1.55% for the $^1P_1^o$ state.

TABLE VI. The $\Delta K_{\rm RNMS}$ (GHz u), $\Delta K_{\rm RSMS}$ (GHz u), and ΔF (GHz/fm^2) factors for the transition $3s^2\,^1S_0$–$3s3p\,^{3,1}P_1^o$.

	$^3P_1^o$–$^1S_0$			$^1P_1^o$–$^1S_0$		
Model	$\Delta K_{\rm RNMS}$	$\Delta K_{\rm RSMS}$	ΔF	$\Delta K_{\rm RNMS}$	$\Delta K_{\rm RSMS}$	ΔF
DF	−614	−844	−0.1944	−615	−129	−0.1945
CV_{1s}-4f	−788	−1646	−0.1915	−911	−732	−0.1921
CV_{1s}-5g	−621	−967	−0.1965	−887	56	−0.1873
CV_{1s}-6h	−647	−943	−0.2025	−957	86	−0.1928
CV_{1s}-7g	−622	−972	−0.2009	−937	46	−0.1911
CV_{1s}-8f	−633	−975	−0.2029	−975	49	−0.1928
CV_{1s}-9f	−632	−975	−0.2028	−978	48	−0.1930
CV_{1s}-10f	−623	−974	−0.2026	−971	49	−0.1927
CV_{1s}-11d	−624	−974	−0.2026	−977	50	−0.1927
CV_{1s}-12d	−623	−974	−0.2026	−977	51	−0.1927
CV_{1s}-13d	−624	−974	−0.2026	−977	51	−0.1927
CC_{2s}	−597	−596	−0.2021	−823	−152	−0.1930
MR_1-8	−617	−771	−0.1928	−841	−112	−0.1890
MR_2-5	−718	−1154	−0.1982	−1064	−452	−0.1916
MR_3-4	−608	−989	−0.1971	−931	−268	−0.1904

B. Isotope shift factors of transitions $3s^2\,^1S_0$–$3s3p\,^{3,1}P_1^o$

Table VI shows the isotope shift factors, including the relativistic normal $\Delta K_{\rm RNMS}$ and specific mass shifts factors $\Delta K_{\rm RSMS}$, and the field shift factors ΔF, for the transitions $3s^2\,^1S_0$–$3s3p\,^{3,1}P_1^o$ as functions of computational models. From this table we can see that the mass shift factors are more sensitive to the electron correlations than the field shift factors, especially for the specific mass shift factors. For instance, from the model DF to CV_{1s}-4f, the change of the $\Delta K_{\rm RNMS}$ reaches 28% for the transition $3s^2\,^1S_0$–$3s3p^3P_1^o$, and 48% for $3s^2\,^1S_0$–$3s3p\,^1P_1^o$. While the $\Delta K_{\rm RSMS}$ reduced by a factor of 2 for the transition $3s^2\,^1S_0$–$3s3p\,^3P_1^o$, and a factor of 6 for the transition $3s^2\,^1S_0$–$3s3p\,^1P_1^o$, respectively. In contrast, the change for ΔF is marginal, less than 2%. The high sensitivity of the SMS factors to the electron correlations is shown again when the CC_{2s} correlations were included in RCI computations. The influences of the CC_{2s} correlation on the $\Delta K_{\rm RNMS}$ is about 16%, and the change is about three times for the $\Delta K_{\rm RSMS}$ of the transition $3s^2\,^1S_0$–$3s3p\,^1P_1^o$. For the transition $3s^2\,^1S_0$–$3s3p\,^3P_1^o$ the effects of CC_{2s} correlation and related higherorder correlation on the isotope shift factors are opposite, which is similar to the case of the hyperfine interaction constants. However, the CC_{2s} and related higher-order correlations both decrease the $\Delta K_{\rm RSMS}$ of the transition $3s^2\,^1S_0$–$3s3p\,^1P_1^o$.

We display the relativistic and nonrelativistic NMS $\Delta K_{\rm RNMS}$ and $\Delta K_{\rm NMS}$, the SMS $\Delta K_{\rm RSMS}$ and $\Delta K_{\rm SMS}$, the FS ΔF factors and their uncertainties (in parentheses) in Table VII for the transitions $3s^2\,^1S_0$–$3s3p\,^{3,1}P_1^o$. In the nonrelativistic approximation, the NMS factors for a given transition are proportional to its transition frequency ν, i.e., the scaling law $\Delta K_{\rm NMS} = -\nu/1823$ [49]. Using the experimental transition energies, we obtained the nonrelativistic normal mass shift factor $\Delta K_{\rm NMS} = -615.67$ (GHz u) for the $3s^2\,^1S_0$–$3s3p$

TABLE VII. The ΔK_{NMS} (GHz u), ΔK_{RNMS} (GHz u), ΔK_{SMS} (GHz u), ΔK_{SMS} (GHz u), and $\Delta F(\mathrm{GHz/fm}^2)$ factors for the transitions $3s^2\,{}^1S_0$–$3s3p\,{}^{3,1}P_1^o$. The numbers in the parentheses are the uncertainties for our results.

Transition	ΔK_{NMS}	ΔK_{RNMS}	ΔK_{SMS}	ΔK_{RSMS}	ΔF
${}^1S_0 - {}^3P_1^o$	−632(87)	−608(86)	−1003(150)	−989(149)	−0.1971(0.0059)
${}^1S_0 - {}^1P_1^o$	−958(37)	−931(36)	−279(132)	−268(127)	−0.1904(0.0038)

${}^3P_1^o$ transition and $\Delta K_{\mathrm{NMS}} = -983.86$ (GHz u) for the $3s^2\,{}^1S_0$–$3s3\mathrm{p}{}^1P_1^o$ transition, respectively. Compared with our *ab initio* calculation, the discrepancies are less than 3%, which due not only to the neglected CC_{1s} and related higher order correlations but also to the relativistic effect in the atomic state wave functions. The linear correlation between the convergency of the calculated transition energy and the MS factors for a given transition has been found in the B^+, C^-, and Cl^- ions [41,50,51], which also occurs in the present case. We deduced from the linear correlation that the SMS factors are changed in a right direction with the MR calculations, since the transition energies in MR_3 model agree better with the experimental value than those in MR_1 and MR_2 models. In addition, from Table VII, it was found that for the transition $3s^2\,{}^1S_0$–$3s3p\,{}^3P_1^o$ the contribution of the relativistic nuclear recoil corrections to the NMS and SMS factors are 24 (GHz u) and 13 (GHz u), respectively. For the other transition, it has similar value. For the total MS factors of the transitions $3s^2\,{}^1S_0$–$3s3p\,{}^{3,1}P_1^o$, the effects of the relativistic nuclear recoil corrections are not more than 4%, which fits our expectation that the relativistic nuclear recoil corrections for ions with $Z = 13$ are small. In addition, we noticed that the effects of the relativistic nuclear recoil corrections on the NMS and SMS factors are insensitive to the electron correlations, which is illustrated in Fig. 2.

For the isotope shift factors, the uncertainties from the VV, $\mathrm{CV}_{1s,}$ and CC_{2s} correlations reach a satisfactory level. Specifically, for the NMS factors of two transitions it is less than 1%, and for the FS factors it is less than 0.1%. The uncertainties of the SMS factors resulting from the VV, $\mathrm{CV}_{1s,}$ and CC_{2s} correlations were controlled less than 2% for the transition $3s^2\,{}^1S_0$–$3s3p\,{}^3P_1^o$ and 7% for $3s^2\,{}^1S_0$–$3s3p\,{}^1P_1^o$. Since the limited computing resource, we cannot further expand the configuration space. Therefore, it is difficult to estimate accurately uncertainties of the mass shift factors in the MR computations due to neglected higher order correlations. Roughly, the uncertainties reach around 8% and 6% for the NMS and SMS factors, respectively, in the $3s^2\,{}^1S_0$–$3s3p\,{}^3P_1^o$ transition. For the $3s^2\,{}^1S_0$–$3s3p\,{}^1P_1^o$ transition, the errors are about 3% for the NMS and 17% for the SMS. Compared with the mass shift factors, the FS factors are stable with expansion of the configuration space. We estimated the uncertainties for the FS factors in the MR calculations to be around 1% for these two transitions. Additionally, we have tested the effects of the CC_{1s} correlation on the IS factors and found that for the NMS factors the uncertainties are not more than 2%, but for the SMS factors they are about 7% and 17% for the $3s^2\,{}^1S_0$–$3s3p\,{}^3P_1^o$ and $3s^2\,{}^1S_0$–$3s3p\,{}^1P_1^o$ transitions, respectively. Nevertheless, the effect of the CC_{1s} correlation on the FS factors is fractional (less than 1%). The Breit interaction corrections to the isotope shift factors, estimated in the DF calculation, are less than 3% for all physical quantities under investigation except for the SMS factors of the $3s^2\,{}^1S_0$–$3s3p\,{}^1P_1^o$ transition to which it is about 7%. To sum up, the total uncertainties are about 14% for the NMS factors, 16% for the SMS factors, and 3% for the FS factor in $3s^2\,{}^1S_0$–$3s3p\,{}^1P_1^o$ transition, and 4%, 47%, and 2% for the other transition. The calculated NMS, SMS, and FS factors together with their uncertainties are listed in Table VII.

V. CONCLUSION

In summery, we calculated the hyperfine interaction constants and the isotope shift factors involving the $3s^2\,{}^1S_0$ and $3s3p\,{}^{3,1}P_1^o$ states in Al^+ ions using the MCDHF method and the active space approach. We have discussed the effects of the electron correlations and the Breit interaction on the atomic parameters concerned. In this case, we found that for the hyperfine interaction constants the contribution of the higher order correlation is opposite with CC correlation. Based on the discussion about the contribution of the electron correlations and the Breit interaction, we have obtained reliable uncertainties for our calculated results. For the hyperfine interaction constants, the uncertainties are less than 1.6%. For the isotope shift factors, the uncertainties are 14% and 4% for the NMS factors, 16% and 47% for the SMS factors, and 3% and 2% for the FS factors in the transitions $3s^2\,{}^1S_0$–$3s3p\,{}^3P_1^o$ and $3s^2\,{}^1S_0$–$3s3p\,{}^1P_1^o$, respectively. Although the higher order correlations change the level structure slightly, these effects on the hyperfine interaction constants and the isotope shift factors are indispensable. Therefore, it is necessary to include the CC correlation and related higher order correlation in computational models in order to achieve high accuracy of atom parameters. In addition, for the Al^+ ion the effect of the relativistic nuclear recoil correction on the mass shift factor is small (less than 4%) and insensitive to the electron correlations.

With respect to the fact that there are relatively large uncertainties in the calculation of mass shift factors, the partitioned correlation function interaction (PCFI) approach [52] will be a promising method for calculating the isotope shifts more accurately, which can capture the different electron correlations flexibly and accurately.

During the review of our article, a paper about hyperfine-mediated electric quadrupole shifts in Al^+ and In^+ ion clocks was published [53]. In this paper, the diagonal magnetic dipole and electric quadrupole hyperfine interaction matrix elements of the $3s3p\,{}^3P_1^o$ state for Al^+ were calculated by using the method of configuration interaction plus many-body perturbation theory (CI+MBPT). For the diagonal magnetic dipole hyperfine interaction matrix element, our value is in perfect agreement with theirs. The consistency is less good for the diagonal electric quadrupole hyperfine interaction matrix element, and the difference is around 35%.

ACKNOWLEDGMENTS

This work has been supported by the National Natural Science Foundation of China under Grants No. 11404025, No. 91536106, No. U1331122, and No. U1530142; the China Postdoctoral Science Foundation under Grant No. 2014M560061; and the Young Teachers Scientific Research Ability Promotion Plan of Northwest Normal University (NWNULKQN-15-3).

---

[1] P. Campbell, I. Moore, and M. Pearson, Prog. Part. Nucl. Phys. **86**, 127 (2016).

[2] X. Z. Cai, H. Y. Zhang, W. Q. Shen, Z. Z. Ren, J. Feng, D. Q. Fang, Z. Y. Zhu, W. Z. Jiang, Y. G. Ma, C. Zhong *et al.*, Phys. Rev. C **65**, 024610 (2002).

[3] T. Nagatomo, H. Ueno, M. Mihara, K. Matsuta, A. Yoshimi, Y. Ichikawa, K. Yamada, H. Kawamura, A. Ozawa, T. Moriguchi *et al.*, Hyperfine Interact. **198**, 103 (2010).

[4] T. G. Cooper, J. Billowes, P. Campbell, and M. R. Pearson, J. Phys. G: Nucl. Part. Phys. **22**, 99 (1996).

[5] V. Kellö, A. J. Sadlej, P. Pyykkö, D. Sundholm, and M. Tokman, Chem. Phys. Lett. **304**, 414 (1999).

[6] D. Sundholm and J. Olsen, Phys. Rev. Lett. **68**, 927 (1992).

[7] I. Angeli and K. Marinova, At. Data Nucl. Data Tables **99**, 69 (2013).

[8] J. M. G. Levins, J. Billowes, P. Campbell, and M. R. Pearson, J. Phys. G: Nucl. Part. Phys. **23**, 1145 (1997).

[9] H. J. Stöckmann, H. Ackermann, D. Dubbers, F. Fujara, M. Grupp, P. Heitjans, and A. Körblein, Hyperfine Interact. **4**, 170 (1978).

[10] D. Nagae, H. Ueno, D. Kameda, M. Takemura, K. Asahi, K. Takase, A. Yoshimi, T. Sugimoto, K. Shimada, T. Nagatomo *et al.*, Phys. Rev. C **79**, 027301 (2009).

[11] D. Kameda, H. Ueno, K. Asahi, M. Takemura, A. Yoshimi, T. Haseyama, M. Uchida, K. Shimada, D. Nagae, G. Kijima *et al.*, Phys. Lett. B **647**, 93 (2007).

[12] T. Nagatomo, K. Shimada, K. Asahi, D. L. Balabanski, J. M. Daugas, M. Depuydt, M. De Rydt, L. Gaudefroy, S. Grévy, Y. Hasama *et al.*, Eur. Phys. J. A **42**, 383 (2009).

[13] M. D. Rydt, G. Neyens, K. Asahi, D. L. Balabanski, J. M. Daugas, M. Depuydt, L. Gaudefroy, S. Grévy, Y. Hasama, and Y. Ichikawa, Phys. Lett. B **678**, 344 (2009).

[14] W. Nörtershäuser, D. Tiedemann, M. Žáková, Z. Andjelkovic, K. Blaum, M. L. Bissell, R. Cazan, G. W. F. Drake, C. Geppert, M. Kowalska *et al.*, Phys. Rev. Lett. **102**, 062503 (2009).

[15] Z. T. Xu, W. H. Yuan, X. Y. Zeng, H. Che, X. H. Shi, K. Deng, J. Zhang, and Z. H. Lu, J. Phys.: Conf. Ser. **723**, 012026 (2016).

[16] E. A. Konovalova and M. G. Kozlov, Phys. Rev. A **92**, 042508 (2015).

[17] J. A. Santana and E. Träbert, Phys. Rev. A **91**, 022503 (2015).

[18] M. Stanek, L. Glowacki, and J. Migdalek, J. Phys. B **29**, 2985 (1996).

[19] U. I. Safronova, W. R. Johnson, and H. G. Berry, Phys. Rev. A **61**, 052503 (2000).

[20] U. I. Safronova, Mol. Phys. **98**, 1213 (2010).

[21] C. Laughlin and G. A. Victor, Astrophys. J. **234**, 407 (1979).

[22] A. Hibbert and F. P. Keenan, J. Phys. B **20**, 4693 (1987).

[23] T. Brage, P. G. Judge, A. Aboussaïd, M. R. Godefroid, P. Jönsson, A. Ynnerman, C. F. Fischer, and D. S. Leckrone, Astrophys. J. **500**, 507 (1998).

[24] P. Jönsson and C. F. Fischer, J. Phys. B **30**, 5861 (1997).

[25] Y. Zou and C. F. Fischer, Phys. Rev. A **62**, 062505 (2000).

[26] Y. Zou and C. F. Fischer, J. Phys. B **34**, 915 (2001).

[27] C. F. Fischer, G. Tachiev, and A. Irimia, At. Data Nucl. Data Tables **92**, 607 (2006).

[28] H. Kang, J. Li, C. Dong, P. Jönsson, and G. Gaigalas, J. Phys. B **42**, 195002 (2009).

[29] H. Kang, J. Li, C. Dong, and G. Gaigalas, J. Phys. B **43**, 095003 (2010).

[30] M. Andersson, Y. Zou, R. Hutton, and T. Brage, J. Phys. B **43**, 095001 (2010).

[31] I. P. Grant, *Relativistic Quantum Theory of Atoms and Molecules* (Springer, New York, 2007).

[32] J. Li, P. Jönsson, M. Godefroid, C. Dong, and G. Gaigalas, Phys. Rev. A **86**, 052523 (2012).

[33] I. Lindgren, Rep. Prog. Phys. **47**, 345 (1984).

[34] P. Jönsson, F. A. Parpia, and C. F. Fischer, Comput. Phys. Commun. **96**, 301 (1996).

[35] C. W. P. Palmer, J. Phys. B **20**, 5987 (1987).

[36] G. Torbohm, B. Fricke, and A. Rosén, Phys. Rev. A **31**, 2038 (1985).

[37] J. Li, M. Godefroid, and J. Wang, J. Phys. B **49**, 115002 (2016).

[38] S. A. Blundell, P. E. G. Baird, C. W. P. Palmer, D. N. Stacey, and G. K. Woodgate, J. Phys. B **20**, 3663 (1987).

[39] L. Filippin, M. Godefroid, J. Ekman, and P. Jönsson, Phys. Rev. A **93**, 062512 (2016).

[40] L. Filippin, R. Beerwerth, J. Ekman, S. Fritzsche, M. Godefroid, and P. Jönsson, Phys. Rev. A **94**, 062508 (2016).

[41] T. Carette and M. R. Godefroid, J. Phys. B **46**, 095003 (2013).

[42] T. Carette, C. Drag, O. Scharf, C. Blondel, C. Delsart, C. Froese Fischer, and M. Godefroid, Phys. Rev. A **81**, 042522 (2010).

[43] M. Andersson, J. Grumer, T. Brage, Y. Zou, and R. Hutton, Phys. Rev. A **93**, 032506 (2016).

[44] P. Jönsson, X. He, C. F. Fischer, and I. Grant, Comput. Phys. Commun. **177**, 597 (2007).

[45] P. Jönsson, G. Gaigalas, J. Biero, C. F. Fischer, and I. Grant, Comput. Phys. Commun. **184**, 2197 (2013).

[46] B. Engels, Theor. Chim. Acta **86**, 429 (1993).

[47] J. Bieroń, C. Froese Fischer, P. Jönsson, and P. Pyykkö, J. Phys. B: At. Mol. Opt. Phys. **41**, 115002 (2008).

[48] N. Stone, At. Data Nucl. Data Tables **90**, 75 (2005).

[49] M. Godefroid, C. F. Fischer, and P. Jönsson, J. Phys. B **34**, 1079 (2001).

[50] Jianpeng Liu, Jiguang Li, and Hongxin Zou, Chin. Phys. B **26**, 023104 (2017).

[51] T. Carette and M. R. Godefroid, Phys. Rev. A **83**, 062505 (2011).

[52] S. Verdebout, P. Rynkun, P. Jönsson, G. Gaigalas, C. F. Fischer, and M. Godefroid, J. Phys. B **46**, 085003 (2013).

[53] K. Beloy, D. R. Leibrandt, and W. M. Itano, Phys. Rev. A **95**, 043405 (2017).